Safe and green Li-ion batteries based on $LiFePO_4$ and $Li_4Ti_5O_{12}$ sprayed as aqueous slurries with xanthan gum as a common binder

Alexandre F. Léonard [1], Nathalie Job

Department of Chemical Engineering – Nanomaterials, Catalysis, Electrochemistry – Liège University (B6a), 4000 Liège, Belgium

Abstract

Li-ion batteries based on $LiFePO_4$ positive electrodes and $Li_4Ti_5O_{12}$ negative electrodes, both processed *via* an aqueous slurry preparation pathway, are presented. In this respect, xanthan gum, a cheap and water-soluble polysaccharide, is shown to be a suitable binder for both electrodes, allowing for a simplified and common preparation method. The electrodes, obtained by spray-coating, show an improved adhesion to the current collectors. The performance of the water-processed electrodes have been investigated in half-cells and compared to similar electrodes prepared upon using PVDF as a binder and N-methyl-pyrrolidone as a solvent. Electrochemical characterizations point to similar performance in terms of (dis-)charge capacities and a good cycling stability. Full-cells based on the obtained electrodes also show stable cycling, with a capacity of ~110 mA.h/g at C/2. The procedure was further extended to the use of stainless-steel as current collectors, with similar results in terms of electrochemical behavior. A relationship was established between the (dis-)charge capacity and the loading of active material for both the positive and negative electrodes, demonstrating the need to take this parameter into account when comparing data in terms of performance of the cells. Finally, the spent electrode substrates can easily be recycled upon immersion in water.

[1] Corresponding author. Phone: +32 4 366 3579 ; e-mail: alexandre.leonard@uliege.be

1. Introduction

In the constant quest towards more sustainability, the energy generated by wind, solar or other renewable sources needs to be used more efficiently. In particular, the match between the intermittent production and the delayed consumption can be achieved upon developing appropriate storage devices [1-2]. Among them, Li-ion batteries, already widespread in portable electronic devices and emerging in transportation, could play a major role in the near future [3]. This results from the high energy and power density of batteries based on the Li-ion technologies. The most common Li-ion batteries in terms of energy density are based on $LiCoO_2$ (LCO) cathodes together with graphitic anodes [4]. Such a combination indeed allows for a large potential difference, but suffers from high cost and toxicity of cobalt [5]. More importantly, safety concerns arise, mainly due to the possible degradation of the electrolyte in such a wide potential window and the low thermal stability of the LCO that could lead to a thermal runaway of the battery [6].

Though improvements have been investigated upon substituting (partially) the Co, together with the implementation of battery monitoring systems (BMS) that avoid conditions leading to instability of the elements, it becomes of interest to work on the safe side upon using more stable cathode and anode active materials [7]. As for the stationary storage, where energy and power density (in terms of mass or volume) of the batteries are submitted to less constraints, the $LiFePO_4$/$Li_4Ti_5O_{12}$ pair becomes of special interest [8]. Indeed, despite the lower potential difference delivered by such a cell (1.9 V), both of these active materials appear to be very stable [9-11]. The positive electrode material $LiFePO_4$ (LFP) has a flat charge/discharge profile at 3.45 V *vs.* Li^+/Li, with a theoretical capacity of 170 mA.h/g and is seen as a stable compound owing to its strong covalent P-O bonds [12]. Moreover, LFP displays an ordered olivine structure that allows for stable cycling, presents no toxicity nor significant environmental issues and, last but not least, is a low cost material compared to LCO [13-14]. The negative electrode material $Li_4Ti_5O_{12}$ (LTO) undergoes Li^+ insertion/deinsertion at a flat voltage plateau of 1.55 V *vs.* Li^+/Li and its theoretical capacity is 175 mA.h/g, near that of LFP [15]. The main advantage of LTO is its “zero-strain” character, meaning that it is the only electrode active material that does not undergo any volume change upon Li^+ insertion-extraction, thereby increasing the longevity of the battery [10, 16-17]. Another important feature is the higher operation potential, above 1 V *vs.* Li^+/Li, that avoids the

formation of a solid electrolyte interphase (SEI), commonly observed for low-potential carbon-based electrodes, and prevents the growth of dendritic metallic lithium [5]. All of these facts contribute to safety and cycle life of the battery, which can compensate for the lower potential delivered by the LFP/LTO pair, especially if stationary storage is considered.

The use of green, non-toxic and safe active materials should however not be counterbalanced by the use of toxic solvents during the electrode manufacture processes. For that reason, and in order to go a step further in a more environmentally-benign and cost-effective approach, we decided to explore the use of aqueous slurries with water-soluble binders in place of the commonly employed PVDF binder and the hazardous N-methyl-pyrrolidone (NMP) solvent [18]. The most widely investigated water-soluble binder is the sodium carboxymethyl cellulose (Na-CMC) – styrene-butadiene rubber (SBR) combination [19]. Numerous studies report the successful use of this binder for both positive and negative electrode active materials for Li-ion batteries, as reviewed by Chou *et al.* [20]. More specifically, a comparative study of using a CMC-rubber based system for both $LiFePO_4$ and $Li_4Ti_5O_{12}$ is reported by Fongy *et al.* [21] as well as Zaghib *et al*. [7]. Other water-soluble binders include for instance hydrocolloids such as guar gum, carrageenan, agar-agar [22], polymers like PAA, PVA, PMA [23-24], sodium alginate [25] or chitosan, tragacanth gum and gelatin [26]. The specific use of water-soluble binders for LFP-based electrodes is further developed in detail by He *et al.* [27]. It should be noted however that, in many cases, the water-compatible binders are used in conjunction with one or more dispersants, adding therefore a useless mass of additional ingredients that are not participating to the electrochemical reaction of the electrochemical storage device.

Another possible water-soluble binder is xanthan gum (XG), a natural polysaccharide secreted by the bacterium *Xanthomonas campestris* and largely used as thickener in the food industry as well as for medicine and cosmetics [27]. Only few studies mention the use of XG as a binder for Li-ion battery active materials. In 2011, Courtel *et al.* compared the use of xanthan gum with carboxymethylcellulose, PEDOT and PVDF on the performances of MCMB carbon graphite anodes [28]. More recently, Wang *et al.* studied in detail the adhesion as well as the electrochemical performance of natural graphite deposited on a Cu foil in presence of this binder [29]. Finally, in 2017, He *et al.* reported the use of xanthan gum as a binder for a LFP electrode active material

[27]. In any of these cases, XG is described as being a promising alternative since the prepared electrodes show improved electrochemical performance in comparison to other organic or water-based binders. The results of adhesion are however divergent in these reports when comparing with PVDF. Moreover, since XG is usually used as thickener for food, the slurries tend to become very viscous, which is the reason why in these studies, its concentration is not exceeding 1 wt.%. Indeed, the dispersion of higher loadings in water leads to the formation of a more solid-like slurry, which in turn becomes difficult to cast onto current collectors when electrodes are to be prepared [28].

The aim of this study is to propose a simplified and green preparation procedure of electrodes for safe $LiFePO_4$/$Li_4Ti_5O_{12}$ batteries by using the xanthan gum as versatile and common binder for both the positive and the negative electrode. In addition, the aqueous slurries need to be fluid enough to process electrodes *via* spray-coating, a technique that combines versatility in terms of surface topography and morphology of the support, easy control of coating thickness and rapid drying under the air flow. This global process is an extension of the concept of paintable batteries introduced by Singh *et al.* [30]. To that aim, fluid inks were prepared upon processing the binder with the conducting carbon additive in order to reduce the interactions between the polysaccharide molecules and dispersing it together with either $LiFePO_4$ or $Li_4Ti_5O_{12}$ in water [31]. The electrochemical performance of the prepared positive and negative electrodes are determined in half-cell assemblies and compared to those prepared *via* classical organic routes. Full-cells have also been assembled from these electrodes, in order to prove the viability of the proposed aqueous route with xanthan gum as a binder to prepare safe and green Li-ion batteries.

2. Experimental

2.1. Processing of electrodes

The anode active material, $Li_4Ti_5O_{12}$ (LTO), prepared *via* the spray-drying method as described by Nakahara, *et al.* [32], was provided by ULiège-GREEnMAT laboratory and used without any further treatment as negative electrode active material. C-coated $LiFePO_4$ (LFP), provided by Prayon-beLife company (Pholicat FE-100) was used as the positive electrode active material.

0.200 g xanthan gum (Binder, Sigma Aldrich) and 0.800 g Carbon Super C65 (Conducting Carbon, Timcal) were mixed in a planetary mill (Fritsch Monomill P6) in stainless-steel jars with 20 stainless-steel balls (diameter 10 mm). Mixing was performed at 400 rpm, 5 × 1 min, 15 s pause and in reverse mode. Then, 0.125 g of this mixture were added to 0.375 g of active material, either $Li_4Ti_5O_{12}$ or $LiFePO_4$, leading to a composition by weight percentage of 75 : 20 : 5 (active material : conducting carbon : binder). This mixture was dried during 1 h at 100°C. 3.6 g of MilliQ water were then added, resulting in a slurry containing 12 wt.% solids, followed by magnetic stirring during 3 h at 1000 rpm. Using an airbrush (Harder & Steenbeck Airbrush Evolution Silverline fPc, 0.4 mm nozzle and needle), the slurry was then sprayed on pre-weighed current collector Cu disks in the case of negative electrode materials (∅ 14 mm, punched from a copper foil, MTI corp.), on pre-weighed current collector Al disks in the case of positive electrode materials (∅ 14 mm, punched from an alimentary Reynolds Al foil) and/or on pre-weighed current collector stainless-steel disks for both types of materials (∅ 15.5 mm, MTI corp.). The coated disks were dried during 2 h at ambient temperature and overnight at 60°C. The weight of active material was determined upon weighing the electrodes after drying and subtracting the mass of the corresponding bare current collector disk. The average mass of active material ranged between 1.0 and 3.0 mg/cm², regardless the active material used. As a matter of fact, the loading can easily be tuned upon changing the sprayed surface for a given volume of slurry. As an example, an average mass of 2.2 mg/cm² is obtained if the above-described volume of ink is sprayed on 30 electrode disks displayed on a surface of 15 cm × 20 cm.

For comparison purposes, the inks with the same composition were prepared using a classical PVDF as a binder and N-methyl-2-pyrrolidone (NMP) as a solvent and sprayed on pre-weighed current collector disks as described above. Finally, LTO-

based negative electrodes were also prepared *via* a conventional method using an organic ink (PVDF and NMP) that was spread on a Cu foil by means of a bar-coater (Elcometer 4340 Automatic film applicator), the opening of the knife being adjusted at 100 µm. After drying at ambient temperature during 3 h and at 60°C overnight, 13-mm disk electrodes were punched from this coating. The mass of active material in this case was obtained upon weighing the obtained electrodes and subtracting the average mass of bare Cu disks of the same diameter.

All the obtained electrodes were then dried at 120°C under vacuum (2×10^3 Pa) during 2 h and transferred to an Ar-filled glove-box (MBraun) for building (half-)cell assemblies.

2.2. Electrode characterization

The structural integrity of the active materials was checked by XRD diffraction (Bruker D8 diffractometer, Cu K-α radiation) on the electrodes after processing. Anodes and cathodes were directly observed by scanning electron microscopy with a Philips XL-20 microscope operated at 10 kV.

To evaluate the electrochemical behavior and performance, the formed electrodes were assembled in coin-cells, with 2 Celgard® separators soaked with 80 µL of electrolyte. For the negative electrodes, the electrolyte was lithium hexafluorophosphate 1 M in an ethylene carbonate:diethyl carbonate:dimethylcarbonate – 1:1:1 mixture, whereas lithium hexafluorophosphate 1 M in an ethylene carbonate:diethyl carbonate – 1:1 mixture was employed for the positive electrodes. Metallic lithium was used as reference- and counter-electrode (half-cell design). Full batteries were assembled in coin cells with 2 Celgard® separators soaked with 80 µL of the same electrolyte as used for the negative electrodes.

The cells were then characterized in galvanostatic cycling mode either on a BioLogic VMP3 multichannel potentiostat or on MTI battery cyclers. The temperature was carefully controlled upon placing the (half-)cells inside a climate chamber regulated at 25°C for the whole electrochemical characterization procedure. Cycling was performed between 2.0 and 4.2 V *vs.* Li^+/Li for the LFP-based electrodes and between 1.0 and 2.5 V *vs.* Li^+/Li for the LTO-based electrodes and the full cells. The applied current densities (C-rates) were calculated assuming the theoretical capacities of 175 mA.h/g for LTO and 170 mA.h/g for LFP. The electrodes used for the full-cells assemblies were chosen such as to match the capacities of both LTO and LFP.

3. Results and discussion

3.1. Ink formation and deposition on current collectors

Solid xanthan gum as such is usually difficult to disperse in water, since a gel forms very quickly [28]. This was checked upon adding 0.025 g of xanthan gum, *i.e.* the quantity corresponding to that used for a slurry preparation, to 3.6 g of MilliQ water, followed by magnetic stirring at 1000 rpm. This results in a gel-like mixture that cannot be processed further. The same experiment was further carried out with the other components needed for a cathode slurry preparation. In this case, 0.025 g xanthan gum binder, 0.100 g conducting carbon, and 0.375 g $LiFePO_4$, were hand-mixed in a vial, leading to a composition by weight percentage of 75 : 20 : 5 (active material : conducting carbon : binder). To this mixture, 3.6 g of MilliQ water were then added, resulting in a slurry containing 12 wt.% solids (the same composition as described in the experimental part for active materials inks preparation), followed by magnetic stirring at 1000 rpm. Again, as for the case of the xanthan gum alone, a gel-like mixture is formed, which cannot be further processed either by spraying or by bar-coater.

On the opposite, in the present case, the xanthan gum binder and the conducting carbon additive were first mixed together by ball-milling. Upon addition of the active material and dispersion in water, a fluid ink can be obtained, which can easily be spread on current collectors either by spray or bar-coating techniques. This observation is quite new since xanthan gum binder can usually only be processed upon using very low-concentration solutions and/or by employing additives such as dispersants, *e.g.* polyethylene imine, to stabilize the formed slurries [27-29]. In the present case, the formation of a solid mixture of xanthan gum and conducting carbon with interactions between both prevents the rapid gelling of the binder and allows for the formation of a stable suspension after processing in water to form an ink. The viscosity of the latter can further easily be modulated upon adjusting the quantity of added water. In the present case, quite liquid inks (or paints) were formed with concentrations ranging between 6 and 12 wt.% solids. Indeed, the aim was to combine the use of a water-soluble binder with the spray technology to coat the current collectors with active materials. This technique presents the advantage in view of the fact that it is a contactless coating process. The surface topography has no influence on the quantity of coated active material and virtually any shape (and nature) of current collector can be covered by an active material. Moreover, the amount of coated material can be tuned from very small to very large quantities, simply by increasing the

total volume of ink sprayed on a given area. Last but not least, when combined with the use of water as a solvent, the applied layers dry very rapidly at ambient temperature, due to the air flow that drives the spraying [20]. This is also of importance since no high temperature treatments are required to manufacture stable and adherent coatings of electrode materials on current collectors.

3.2. Structural and morphological characterizations

The structural integrity of the two active materials was checked after being processed into electrodes *via* our innovative water-based pathway. The XRD patterns (Figure S1) clearly indicate that neither the LTO, nor the LFP were altered, with all the diffraction lines of the corresponding crystal structures being present, in addition to those of the Cu or Al supports, respectively. In addition, the diffraction patterns are quite in line with those reported for similar materials [17, 33].

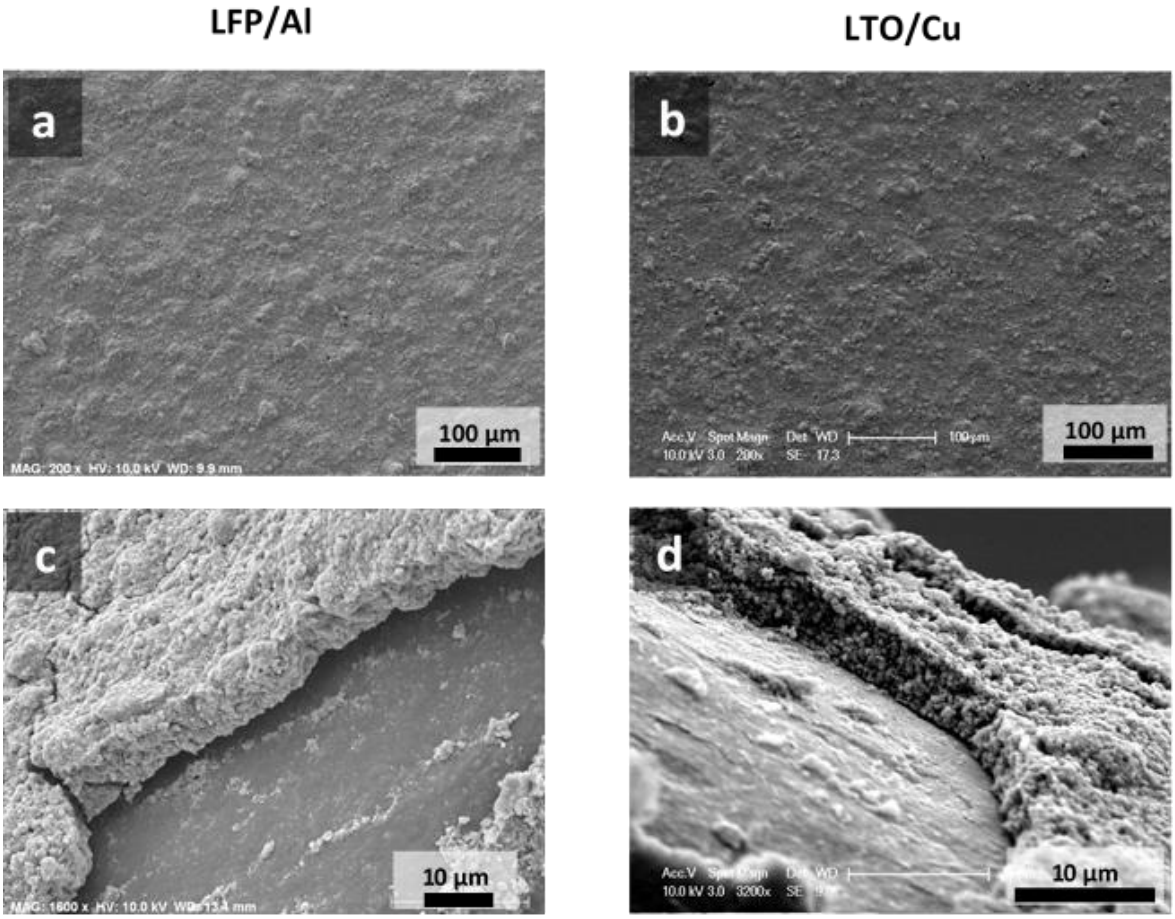

Figure 1: SEM images of $LiFePO_4$/Al electrodes (a, c) and $Li_4Ti_5O_{12}$/Cu electrodes (b, d) at different magnifications.

The electrodes were visualized by scanning electron microscopy (Figure 1). Low-magnification observations show homogeneous coatings over the whole surface of the Al or Cu disks, with some small cracks that merely result from the manipulation of the electrodes. Side-observations at higher magnification also show the homogeneity of the coating, with well-dispersed particles of active material in presence of the conducting carbon additive and the xanthan gum binder. The thickness of the coatings could be estimated to range between 5 and 8 µm in this case, for electrode loadings of 1.3-1.5 mg/cm^2, independently of the active material used.

3.3. Adhesion of the active materials

The adhesion of the coatings was evaluated by using the ASTM D3359-97 procedure, also known as Scotch tape test [34]. This test is based on the application of an adhesive paper on the surface and peeling it off at an angle of 180°. The adhesion is then quantified upon observing the substrate and determining the percentage of area removed after delimiting the surface into small squares separated by parallel cuts. The percentage of affectation was however impossible to determine in the present case, since the coatings were homogeneously removed instead of flaking along edges or being removed from (some) whole squares. Nevertheless, is was possible to qualitatively evaluate the comparative adhesion of the coatings upon observing the substrate and, more particularly, the adhesive paper by transparency.

For that purpose, three coatings have been compared: (i) $Li_4Ti_5O_{12}$ prepared *via* an aqueous slurry in presence of xanthan gum as a binder and sprayed on a Cu foil, (ii) the same ink spread by bar-coater and (iii) an organic ink with PVDF as a binder and NMP as solvent, processed by spray.

Table S2 shows the photographs of the coatings (left) and the adhesive paper (right) after the adhesion test. Clearly, the combination of a water-based slurry with spraying leads to coatings that display an improved adhesion to the substrate, since more active material remains present on the Cu foil and much less is present on the adhesive tape. Similar observations were further done for the same test performed on positive electrodes with $LiFePO_4$ coated on Al with different techniques and an aqueous or organic slurry preparation method.

3.4. $Li_4Ti_5O_{12}$ electrochemical performance in half-cells

Table 1: Discharge capacity at cycles 1, 10 and 20 of LTO-based anodes processed *via* different pathways and cycled at a rate of C/5 (5 h to fully discharge the half-cell).

	$Q_{disch.}$ (1) (mA.h/g)	$Q_{disch.}$ (10) (mA.h/g)	$Q_{disch.}$ (20) (mA.h/g)
PVDF/NMP – bar-coater	167	166	166
PVDF/NMP – spray	163	159	159
Xanthan gum/Water – spray	162	162	162

The behavior of $Li_4Ti_5O_{12}$ electrodes processed using xanthan gum as a binder and water as a solvent was compared to that of the same negative electrodes prepared *via* a more classical route, *i.e.* using PVDF as a binder and dispersing the solids in NMP. From these latter slurries, both the bar-coating and spraying techniques were used.

A typical charge-discharge curve (not shown here) displays a flat operating voltage at ~1.5 V, corresponding to the reversible two-phase reaction of Li (de-)insertion following the reaction: $Li_4Ti_5O_{12} + 3Li^+ + 3e^- \leftrightarrow Li_7Ti_5O_{12}$.

As seen from Table 1, very similar values of capacity are recorded during the first 20 charge-discharge cycles at a rate of C/5, independently of the preparation method. The cycling stability also remains the same in each case, with a capacity after 20 cycles that stays at 93-95 % of the theoretical capacity of LTO (175 mA.h/g).

Figure 2 compares the evolution of capacity upon cycling at variable rates up to 10C (6 min to fully discharge the half-cell) for the aqueous (spray) and organic (bar-coater and spray) pathways used to prepare the electrodes. Table 2 summarizes the associated numerical values.

Table 2: Discharge capacity of LTO-based anodes processed *via* different pathways at different cycling rates from C/5 to 10C.

	Discharge capacity (mA.h/g)					
	C/5	**C/2**	**1C**	**2C**	**5C**	**10C**
PVDF/NMP – bar-coater	166	163	160	143	104	70
PVDF/NMP – spray	173	170	164	146	95	52
Xanthan gum/Water – spray	162	159	143	133	66	30
Xanthan gum/Water – spray ***Modified route***	174	171	167	159	137	99

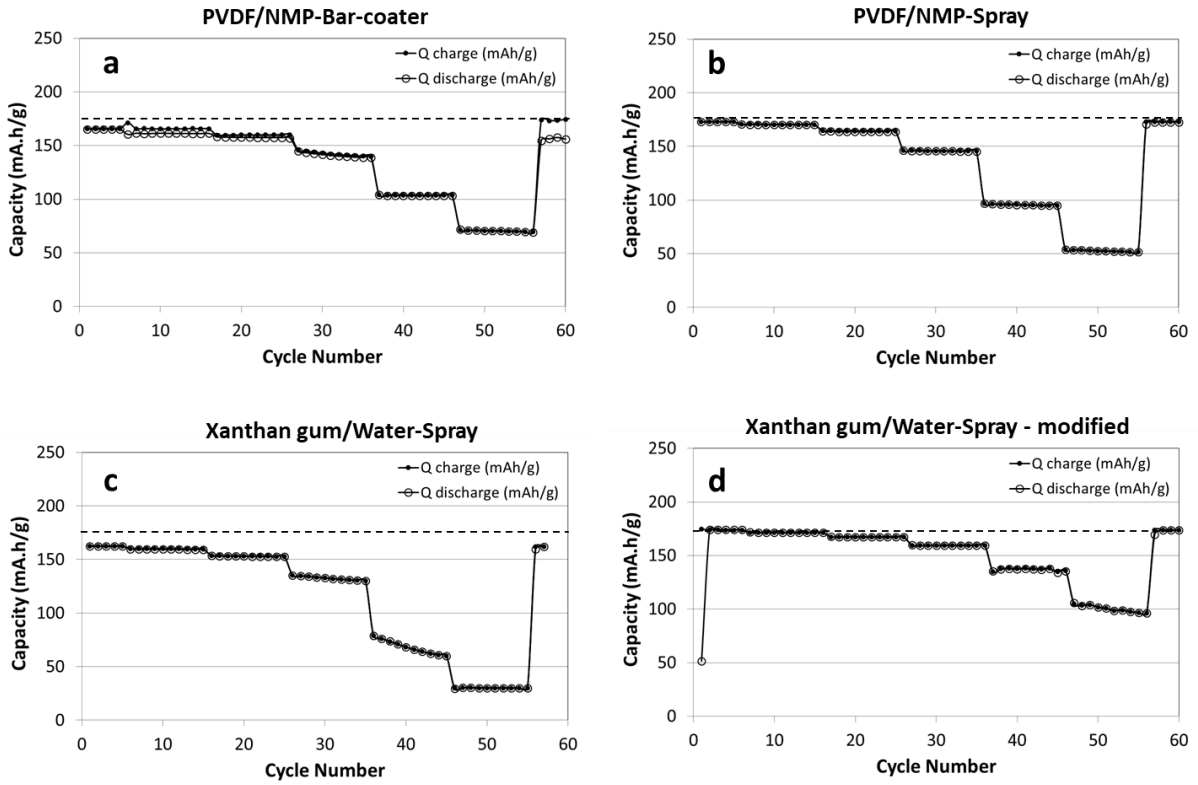

Figure 2: Evolution of (dis-)charge capacity of LTO-based electrodes processed *via* different pathways at different cycling rates from C/5 to 10C. (a, b) : Organic slurries, (c, d) : aqueous slurries. The horizontal dotted line represents the theoretical capacity of LTO (175 mA.h/g).

The global behavior is the same for the LTO-based electrodes, regardless the preparation pathway, with a decrease in specific capacity upon increasing the cycling rate. Considering the water-based pathway with xanthan gum as a binder, somewhat lower values of specific discharge capacities are recorded, especially if cycling is performed at very high current densities (Table 2 and Figure 2c). Such a behavior could very well be attributed to limitations in terms of electronic conductivity that would become more important as the imposed current becomes higher. For that reason, a modified water-based processing pathway was explored. In order to improve the contact between the insulating $Li_4Ti_5O_{12}$, the binder and the conducting carbon additive, all of these constituents were mixed together by ball-milling, instead of just mixing the binder and the carbon, leading to the 'modified route', as labelled in Table 2 and Figure 2d. The obtained solid mixture was then dispersed in water to prepare a slurry as for the unmodified route, resulting in a liquid ink that could easily be sprayed on current collector disks.

As seen from Table 2 and Figure 2d, the recorded discharge capacities are much higher in this case, with values near that the theoretical capacity at C/5 and up to 99 mA.h/g when cycling is performed at 10C. Furthermore, the initial capacity is fully recovered when turning back to C/5 again. Also, the electrodes processed *via* this modified water-based route outperform those prepared with PVDF and NMP as organic solvent. It is worth mentioning here that the mass of active material could be determined with a high precision since the spraying procedure allows for weighing the Cu disks before and after coating with active material, which is not the case when the bar-coater procedure is employed. Indeed, we could evidence quite significant inhomogeneity in the used Cu foil, with mass variations up to 5 %. This discrepancy could then in turn strongly affect the calculated values of specific capacity.

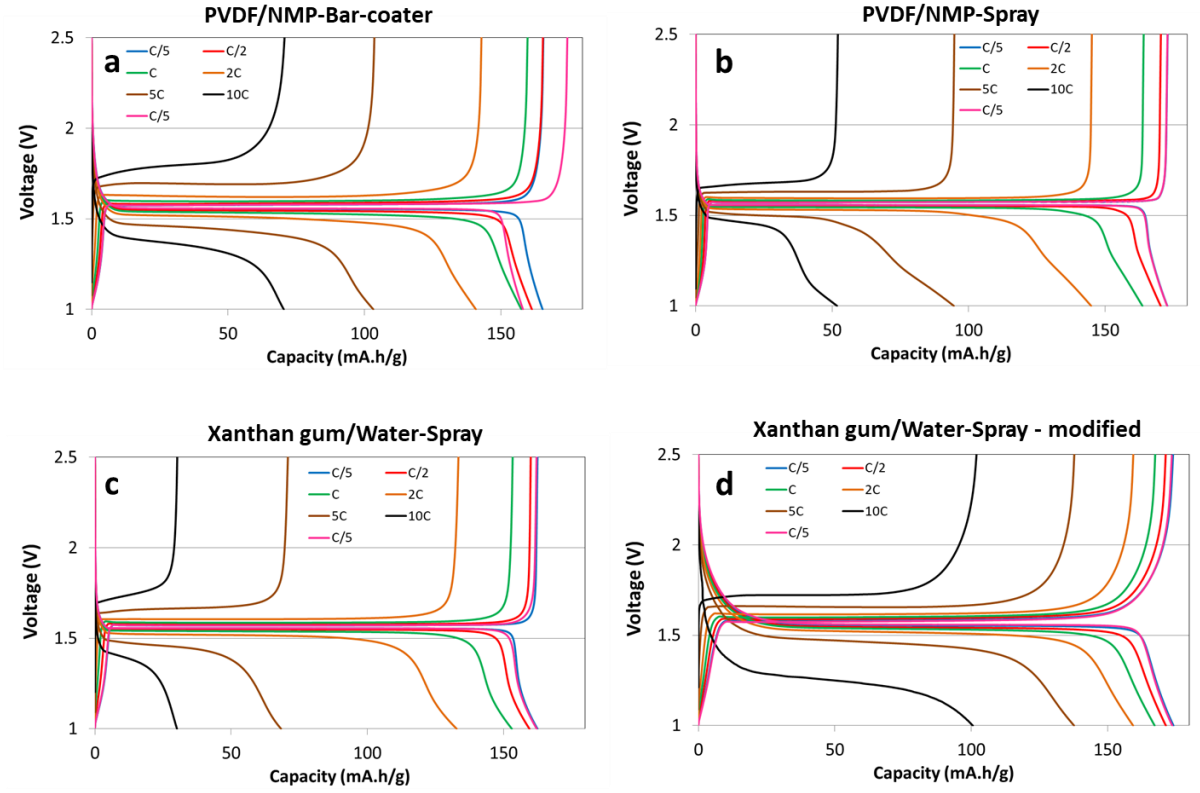

Figure 3: Voltage-capacity curves of LTO-based electrodes processed *via* different pathways at different cycling rates from C/5 to 10C. (a, b) : Organic slurries, (c, d) : aqueous slurries.

In addition to comparing the absolute values of discharge capacities, the evolution of the voltage profiles as a function of capacity also needs to be taken into account. As can be highlighted from Figure 3, the recorded profiles show some differences. In

particular, despite their higher capacity at each rate, the electrodes prepared *via* the modified aqueous pathway show more sloping charge and discharge profiles, indicating that the full capacity is stored or delivered over a wider potential window. This is also the case (although to a lesser extent) for the electrodes obtained after coating an organic ink by the bar-coater technique. Such profiles are less appropriate for real battery applications, where the capacity should be delivered at a constant voltage. Moreover, the plateaus, at which insertion and deinsertion occur, are more split in these two cases, suggesting a more pronounced overpotential resulting from kinetic limitations in Li^+ insertion/extraction. The electrodes processed *via* an organic ink and spray processing show a steep charge, but a hump is visible at the end of discharge, which becomes more pronounced as the applied current density becomes higher. Finally, though the discharge capacities remain lower at high rates, it seems in the present case that the LTO electrodes processed with xanthan gum *via* the unmodified aqueous route show the most appropriate charge and discharge profiles.

Cycling stability of such electrodes was further verified upon applying a program consisting of 20 cycles at C/5, 100 cycles at 1C, followed by 3 sequences of variable rate cycling up to 10C. The resulting capacity curves are represented in Figure 4.

The LTO-based electrodes show a very good cycling stability, with recovery of capacity even after cycling several times at a rate up to 10C.

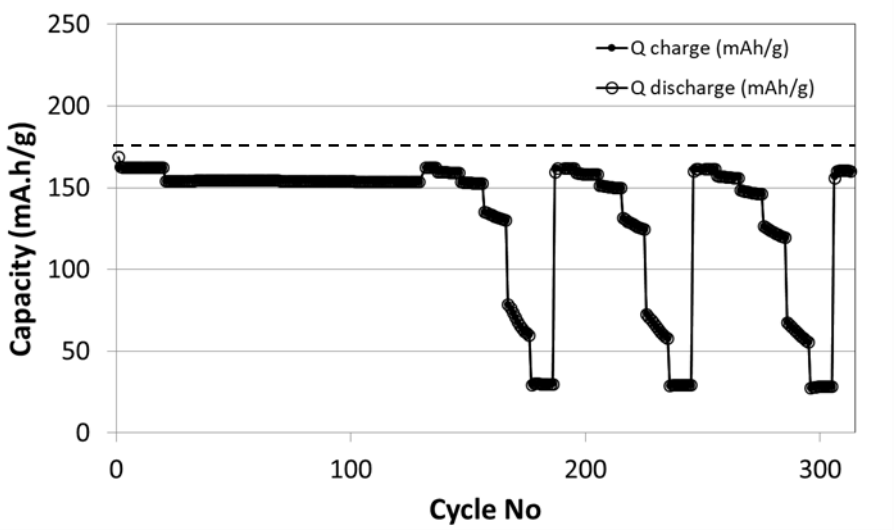

Figure 4: Capacity as a function of cycle number for an LTO-based electrode processed *via* the initial aqueous route and cycled at C/5, 1C, followed by 3 sequences at C/5, C/2, 1C, 2C, 5C and 10C. The horizontal dotted line represents the theoretical capacity of LTO.

The composition of the aqueous slurries was further modified upon increasing the relative fraction of conducting carbon additive, leading to a composition by mass percentage of 70 : 25 : 5 (active material : conducting carbon : binder) in order to determine whether the high-rate performance could be improved by enhancing the electron conductivity. The obtained values of discharge capacity as a function of cycling rate for two half-cells of each composition are given in Table 3. The results obtained in this case show similar splitting between insertion and de-insertion plateaus, as well as values of capacity that remain in the same range. From the point of view of performance, there is thus no point in increasing the quantity of conducting carbon, since it adds a mass to the electrode that will not take part in the electrochemical reaction. Nevertheless, the obtained results illustrate quite well the versatility of the proposed aqueous processing route.

Table 3. Discharge capacity of LTO/Cu electrodes prepared *via* an aqueous slurry and with different LTO:C wt.% ratios at different cycling rates up to 10C.

		Discharge capacity (mA.h/g)					
LTO wt.%	**Sample #**	**C/5**	**C/2**	**1C**	**2C**	**5C**	**10C**
75	**1**	162	159	151	128	65	30
	2	159	156	147	122	62	30
70	**1**	153	149	141	119	62	31
	2	153	151	143	121	62	31

All of the obtained results clearly show that LTO-based electrodes, designed as negative electrodes for Li-ion batteries, can be prepared upon using a water-soluble binder, without need of any other additives such as stabilizers or dispersants. Electrodes with performances near those recorded for classical organic-based systems can thus be obtained *via* a simple and water-based approach combined with the versatile spraying coating process.

3.5. $LiFePO_4$ electrochemical performance in half-cells

The transferability of the previously developed processing route was further evaluated for electrodes based on $LiFePO_4$. As mentioned in the introduction part, $LiFePO_4$ displays a theoretical capacity of 170 mA.h/g, with a flat insertion plateau at about 3.5 V *vs.* Li^+/Li. As in the case of the LTO electrodes, the performance of LFP processed as an aqueous slurry with xanthan gum as a binder was compared to that of electrodes prepared *via* an organic medium with PVDF and NMP.

The modified aqueous pathway as described above, *i.e.* upon mixing all constituents (LFP, conducting carbon, binder) by planetary mill prior to dispersion in water, was investigated in a first instance. The electrochemical characterizations realized in half-cells revealed a rapid fade in capacity upon cycling, even at low rates. This observation could find its explanation in the employed process. Indeed, the commercial LFP particles are initially covered by a thin carbon layer (2.14 wt.% in total) that ensures a sufficient electron conductivity. In this case, the ball-milling process could very well break apart this layer, thereby strongly reducing the conductivity of the LFP that would not be compensated by the conducting carbon present in the electrode preparation slurry. This route was thus abandoned and the initial preparation pathway, *i.e.* mixing the xanthan gum with the conducting carbon by ball-milling, followed by the addition of the active material, was used instead for the further studies.

Figure 5 compares the charge and discharge capacity as a function of cycle number for the LFP electrodes prepared *via* the aqueous and organic routes, both realized by spray coating. The corresponding voltage–capacity curves at each rate of cycling are also illustrated and the numerical values of discharge capacity are given in Table 4.

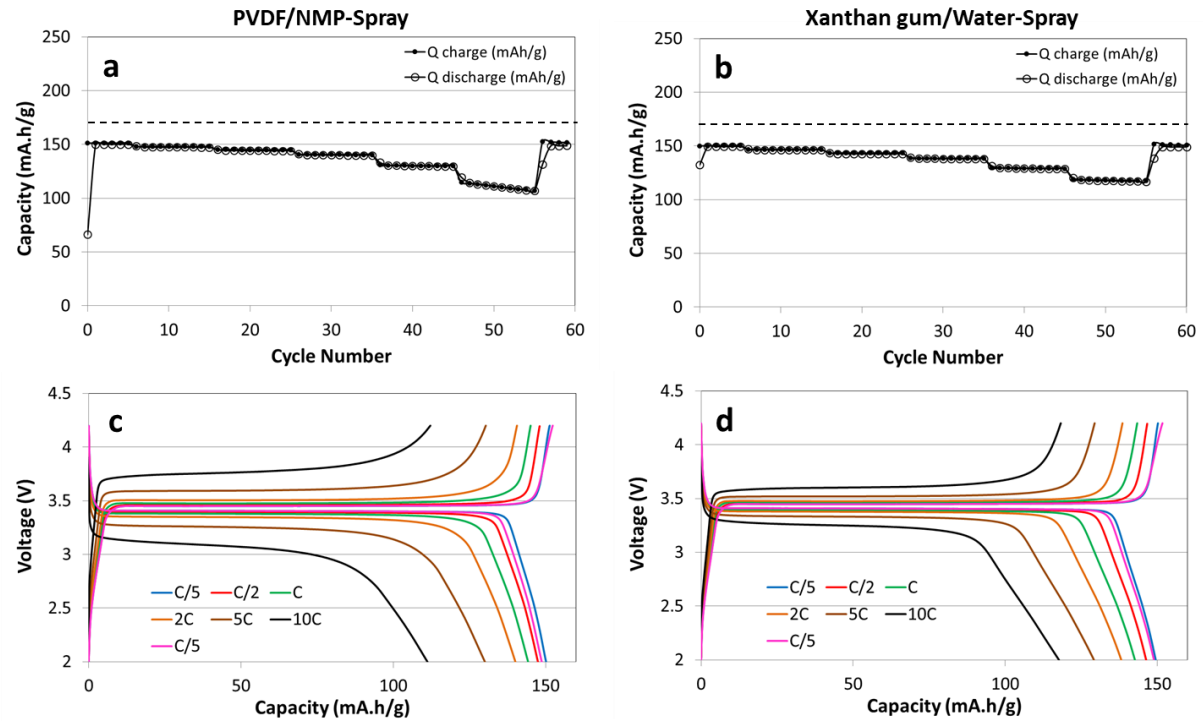

Figure 5: Evolution of (dis-)charge capacity (a, b) and corresponding voltage-capacity curves (c, d) of LFP-based electrodes processed *via* different pathways at different cycling rates from C/5 to 10C. (a, c) : Organic slurries, (b, d) : aqueous slurries. The horizontal dotted line represents the theoretical capacity of LFP (170 mA.h/g).

Table 4: Discharge capacity of LFP-based electrodes processed *via* different pathways at different cycling rates from C/5 to 10C.

	Discharge capacity (mA.h/g)					
	C/5	**C/2**	**1C**	**2C**	**5C**	**10C**
PVDF/NMP – spray	150	147	144	140	130	110
Xanthan gum/Water – spray	150	146	143	138	129	118

The values of discharge capacity are very similar, independently of the preparation pathway, and in line (though somewhat lower, but no details were given regarding the testing procedure) with those reported in the specification sheet of the commercial LFP. Capacities up to 118 mA.h/g can even be reached at a cycling rate of 10C (6 min for a full (dis-)charge) in the case of the electrodes prepared with xanthan gum as a binder. The voltage-capacity curves clearly show the insertion/deinsertion flat profile centered on about 3.5 V at the low cycling rates and corresponding to the reaction: $LiFePO_4 \leftrightarrow FePO_4 + Li^+ + 1e^-$. As for the $Li_4Ti_5O_{12}$ anodes, the plateaus tend to split with the applied

cycling rate, but reversibly come back to the initial value when cycling is carried out at C/5 again, as proven by the superimposed curves at this rate. Interestingly, this splitting seems less pronounced for the electrodes processed in water.

The cycling stability of the water-processed LFP electrodes was further verified upon applying a program consisting of 20 cycles at C/5, 100 cycles at 1C, followed by 3 sequences of variable rate cycling up to 10C. The resulting capacity curves as a function of cycle number are represented in Figure 6.

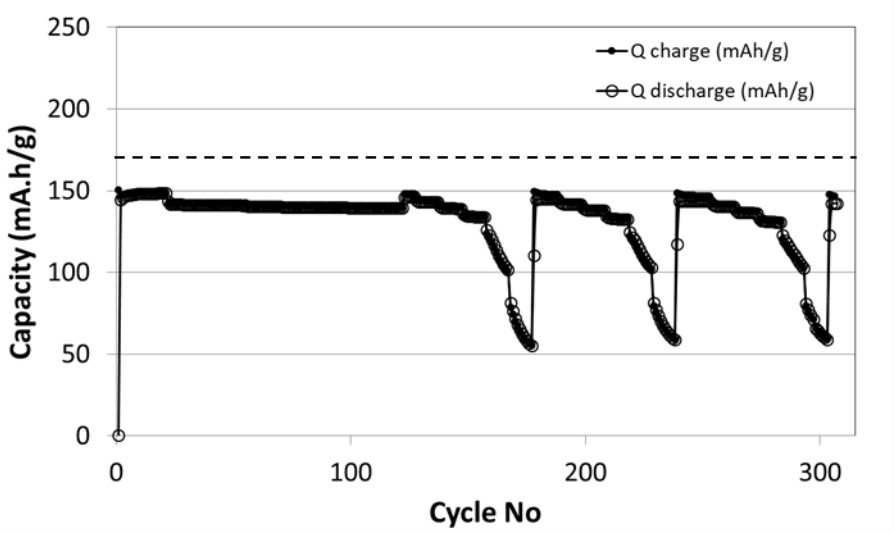

Figure 6: Capacity as a function of cycle number for a LFP-based electrode processed *via* an aqueous route and cycled at C/5, 1C, followed by 3 sequences at C/5, C/2, 1C, 2C, 5C and 10C. The horizontal dotted line represents the theoretical capacity of LFP.

The as-processed electrodes clearly show a very good cycling stability, with stable values of (dis-)charge capacity at each cycling rate. As for the LTO-case, the water-based route thus seems to be a very promising alternative in the processing of positive electrode materials for Li-ion batteries.

A further study was carried out upon increasing the relative amount of added conducting carbon additive up to 25 wt.%, the quantity of binder remaining the same (5 wt.%). Two different electrodes of each composition were tested for the sake of reproducibility.

Table 5. Discharge capacity of LFP/Al electrodes prepared *via* an aqueous slurry and with different LFP:C wt.% ratios at different cycling rates up to 10C.

LFP wt.%	Sample #	Discharge capacity (mA.h/g)					
		C/5	C/2	1C	2C	5C	10C
75	1	144	138	134	128	103	37
	2	148	143	139	134	105	41
70	1	144	140	136	131	109	52
	2	145	142	138	130	80	37

A seen from Table 5, the discharge capacity at each cycle rate remains in the same range, independently of the relative amount of conducting carbon present in the ink. This is consistent with the observations made for the LTO-based electrodes processed in the same manner, and demonstrates the versatility in terms of ink compositions for the proposed aqueous preparation pathway.

When comparing the data regarding discharge capacity between Tables 4 and 5, a discrepancy can be noted regarding the values measured for the cycling rates above 1C. This difference can be explained by the fact that electrodes with different loadings of active materials have been used in the different experiments, which is explained in more details below.

3.6. Influence of the mass of active material on the electrochemical performance of LTO- or LFP based electrodes.

As mentioned above, a decay in the values of discharge capacities has been observed with the increase in the loading of active material. In order to further highlight this tendency, the measured discharge capacity of a large series of LFP-based electrodes, prepared *via* the water-based coating procedure, was plotted as a function of the mass of active material, for different cycling rates. As shown in Figure 7a, a stable capacity of about 138 mA.h/g is obtained if the cycling rate is carried out at 1C, independently of the loading of LFP on the electrode between 2.3 and 5.2 mg. If cycling is carried out at higher rates, from 2C to 10C, a clear inverse relationship can be evidenced between the capacity and the mass of active material. Since the applied cycling rate was calculated upon using the theoretical capacity of LFP (170 mA.h/g), the higher masses also correspond to higher applied current densities.

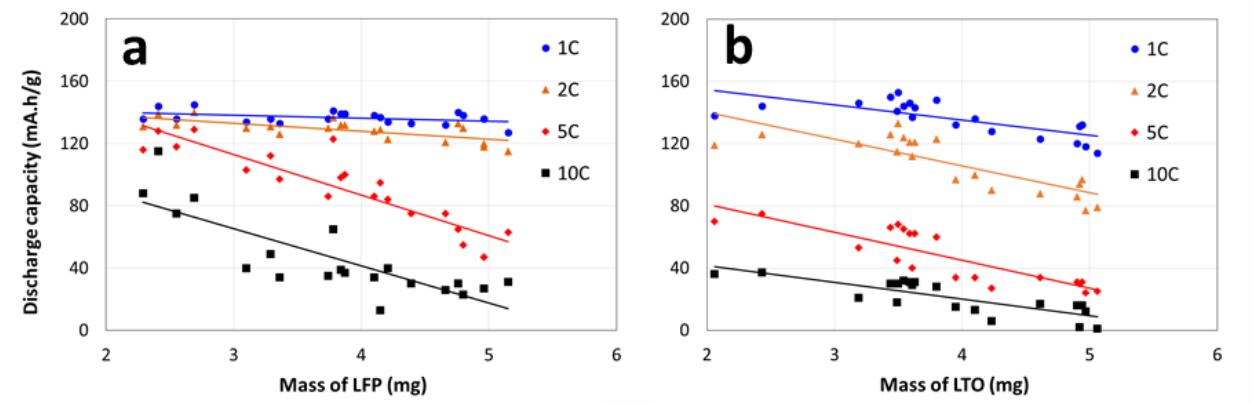

Figure 7: Discharge capacity as a function of the mass of active material on the electrode for LFP-based electrodes (a) and LTO-based electrodes (b), at different cycling rates (1C, 2C, 5C and 10C).

The decay in charge and discharge capacities with the applied current could result from electronic conductivity or ionic diffusion issues within the electrode body. It should be mentioned that no pressing step was applied on the electrodes after coating and prior to half-cell assembly. The same observations were made on the LTO-based electrodes processed in the same manner as the LFP-based ones (Figure 7b). In this case, a decay already takes place at a cycling rate of 1C, whereas a constant capacity was recorded at C/5 and C/2 (data not shown on Figure 7b for the sake of clarity). The different behavior could be explained by the fact that the $Li_4Ti_5O_{12}$ has a more insulating character than the C-coated $LiFePO_4$ particles. The electron conductivity between the particles within the electrode body is thus only ensured by the conducting carbon additive, which is present in the same ratio for both the electrode types. The fact that the overall conductivity in the LTO-based electrodes is lower could thus account for the worse performance at higher cycling rates. AC impedance measurements have been carried out on several LFP- and LTO-based electrodes processed *via* the proposed aqueous route. From a general point of view, the charge transfer resistance (R_{ct}), calculated form the semicircle at high-middle frequency on the Nyquist plot, remains lower for the C-coated LFP electrodes in comparison to the LTO anodes. This is also in line with the trends observed by Gao *et al.*, though the R_{ct} values in our case were much lower (20-40 Ω *vs.* 93-290 Ω for $LiFePO_4$ and 80-140 Ω *vs.* 300-1600 Ω for $Li_4Ti_5O_{12}$) [11].

The presented results highlight the importance of considering the mass of active material (or the applied absolute charge and discharge currents) when comparing data between each other. This was taken into account in the previous sections of this manuscript, where the electrodes, processed either in organic or aqueous media, all bore a similar loading of LTO or LFP. Also the comparison of data from literature in general should take into account this influence, observed at least in the present conditions of electrode processing.

3.7. Diversification of current collectors: LFP or LTO on Stainless-Steel substrates

In addition to using a single preparation route of the slurries for both the negative and positive electrode active materials, a step further consisted in investigating the use of the same current collector on both sides of a battery. As a matter of fact, the use LFP and LTO allows for operation in a more restricted potential window, so that the current collectors will not undergo oxidation processes on their surface. Stainless-steel (SS) disks have been used in a first instance for that purpose and the results of cycling on two electrodes (two different coatings) of each kind are given in Table 6.

The values of discharge capacity are fully in line with those recorded on Al and Cu current collector disks for the positive and negative electrodes respectively (see Tables 3 and 5). Note that the masses of active material were in the same range for each of the samples, with an average value of about 5.0 mg.

Table 6. Discharge capacity of LFP/SS and LTO/SS electrodes prepared *via* an aqueous slurry, at different cycling rates up to 10C.

		Discharge Capacity (mA.h/g)					
	Sample #	**C/5**	**C/2**	**1C**	**2C**	**5C**	**10C**
LFP	**1**	141	140	137	119	81	37
	2	142	140	135	123	73	41
LTO	**1**	155	148	137	106	40	18
	2	154	150	140	116	59	29

The data are further in accordance with the capacities obtained for such electrode loadings and as plotted in Figure 7. The good behavior on stainless-steel disks is however not a surprise, since the coin-cell cases and internal components are made of this same material, and are designed such as to resist to the electrochemical characterization conditions. The obtained results nevertheless will serve as a baseline for an ongoing study on the use of lower-value steels that could supplant the use of expensive substrates. Indeed, the combination of a simple, inexpensive and unique water-based process for electrodes manufacture with lower-value current collectors could advantageously decrease the fabrication costs of such Li-ion batteries.

3.8. Full batteries assembled from positive and negative electrodes processed via aqueous slurries

The presented LFP- and LTO-based electrodes were assembled in full cells, by taking care to balance the capacities of the positive and negative electrodes. Figure 8a and b represents the (dis-)charge capacity as a function of cycle number for two full cells, the first one with Al and Cu as positive and negative current collectors respectively, the second one with coatings deposited on stainless steel at both sides. The batteries were cycled first at C/10 for 20 cycles, then at C/2 for 100 cycles and finally, the rate-behavior was evaluated upon cycling between C/10 up to 5C. For this latter sequence, the corresponding voltage-capacity profiles are given also (Figure 8c and d).

At low cycling rates, a stable capacity of 135 mA.h/g $_{LFP}$ is obtained. The calculation is based on the limiting electrode, which was chosen to be LFP in the present case, so that all the capacities are expressed as per gram of LFP. The value is somewhat lower than that reported in literature, where values up to 150 mA.h/g are obtained at a similar cycling rate, but with lower loadings than in the present case (2.0 mg/cm² *vs*. 2.6 mg/cm²) [8]. The voltage-capacity profile shows a plateau at ~1.9 V, indicative of the two-phase lithium insertion/de-insertion occurring at both the negative and positive electrodes. If the cycling rate is increased at C/2, the capacity stabilizes at 110 mA.h/g $_{LFP}$ and this value is kept after 100 cycles.

Increasing the cycling rate leads, as for the individual electrodes, to a decay in the measured discharge capacity as expressed in Table 7. The capacity is nevertheless recovered upon returning at a rate of C/10.

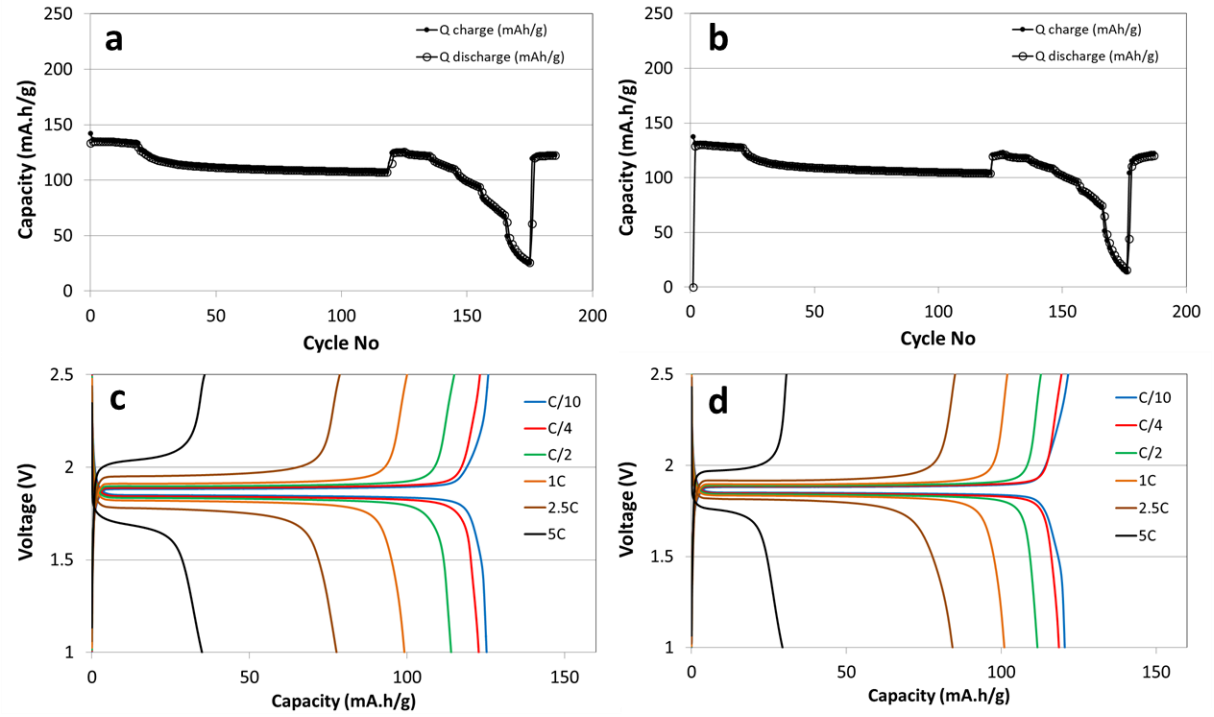

Figure 8: Evolution of (dis-)charge capacity (a, b) and corresponding voltage-capacity curves (c, d) of LFP-LTO full cells at different cycling rates from C/10 to 5C. (a, c) : Al and Cu as current collectors, (b, d) : Stainless steel as current collectors. The capacity is expressed as mA.h/g of LFP contained in the cathode.

Table 7. Discharge capacity of LFP-LTO full cells with Al and Cu or stainless steel as current collectors, at different cycling rates up to 5C. The capacity is expressed as mA.h/g of LFP contained in the cathode.

	Discharge Capacity (mA.h/g)					
Current collectors	**C/10**	**C/4**	**C/2**	**1C**	**2.5C**	**5C**
Al & Cu	125	123	114	99	78	35
SS	120	119	112	101	84	29

Interestingly, the splitting between the charge and discharge plateaus remains quite low, even when cycling at 5C (Figure 8c and d). Values of 0.20 to 0.35 V overpotential are observed in this case, which is in line with data reported for similar full cells with electrodes bearing the same loadings of active materials [8], and lower than observed for heavier electrodes [10], both processed *via* an organic ink. Finally, when comparing the data from Table 7, no difference can be highlighted regarding the use of Al and Cu

or stainless steel as current collectors, which is in line with the characterizations of the individual electrodes in half-cells.

3.9. Recycling of current collectors from used half-cells

A final advantage of the water-based processing route was highlighted upon recovering the current collectors (Al, Cu and stainless steel) from half-cells after the electrochemical characterization procedures. For that purpose, the spent half-cells were disassembled inside the glovebox ant the positive and negative electrodes were recovered from the assemblies. The electrodes were then covered with 3 g of water in small vials. The latter were either shaken by hand or submitted to ultrasound stirring during 10 s. As illustrated in Figure S3, the active material-conducting carbon-binder composites are easily detached from the surface of the current collector disks in each case. After this separation, the current collector disks display an appearance identical to that of their initial state, *i.e.* before being coated to manufacture electrodes. It should be noted here that the volume of added water was chosen arbitrarily, and could very well be reduced. This simple and rapid process to recover and recycle current collectors after the end-of-life of a battery could present a high advantage in the quest towards more eco-friendly processes for electrodes manufacturing. In particular, the use of water for the separation was rendered possible through the presence of the water-soluble xanthan gum as binder for the electrodes preparation.

4. Conclusions

Xanthan gum was evaluated as a versatile and common binder for the preparation of water-based slurries for $Li_4Ti_5O_{12}$ negative electrodes and $LiFePO_4$ positive electrodes, without need of any further additives such as dispersants or stabilizers. A unique preparation route, based on processing aqueous slurries by the spray coating technique, was developed, leading to electrodes that display an improved adhesion to the current collectors. Homogeneous coatings with an excellent retention of the crystalline structure of the active materials were obtained by that means. When characterized in half-cells, these electrodes show comparable performance than those processed *via* a conventional organic pathway with PVDF as a binder and NMP as solvent. A very good cycling stability could further be evidenced, even after cycling at rates up to 10C. A decay in terms of discharge capacity with the loading of active material could however be highlighted, especially when high-rate cycling is considered.

This behavior can probably be related to resistivity issues within the electrode bodies and needs to be taken into account when comparing data between each other. The versatility of the proposed water-based processing route was further demonstrated upon changing the relative amounts of active material and conducting carbon additive. Full-cells were further assembled from the obtained electrodes. Again, a good cycling stability was observed with a capacity of ~110 mA.h/g $_{LFP}$ at a cycling rate of C/2. Stainless steel was evaluated as current collector for both the positive and negative electrodes. The electrochemical characterization in half- and full-cells demonstrate similar performances in terms of (dis-)charge capacity and cycling stability when compared to Al and Cu. Finally, the current collectors of 'used' cells can easily be recovered and recycled, simply upon being covered with water, that allows for a rapid separation of the composite material from the substrate.

The results issued from this study pave the way towards the easy and environmentally-friendly manufacture of safe Li-ion batteries based on the $LiFePO_4$-$Li_4Ti_5O_{12}$ chemistry, especially for the application in stationary energy storage. Further work is currently in progress in order to determine the influence of a calendaring step on the overall performance. Also, the transferability of the proposed route towards other electrode active materials for Li-ion batteries is under investigation.

Acknowledgements

This work was carried out within the framework of the BATWAL project (Région Wallonne, grant agreement 1318146, PE Plan Marshall 2.vert). We thank Mr. Sébastien Caes, from the GreenMat laboratory, for his help in the characterization of electrodes by microscopy. The authors also thank the University of Liège (Fonds Spéciaux pour la Recherche FSR C13/09) and the Fonds de Bay for their financial support.

References

[1] K.P. Kairies, D. Magnor, D.U. Sauer, Energy Procedia 73 (2015) 200-207.

[2] S. Pacala, R. Socolow, Science 305 (2004) 968-971.

[3] J.M. Tarascon, M. Armand, Nature 414 (2001) 359-367.

[4] R. Vasant Kumar, T. Sarakonsri in: *High Energy Density Lithium Batteries*, K.E. Aifantis, S.A. Hackney, R. Vasant-Kumar (eds) Wiley-VCH Verlag GmbH|Co. KGaA, Weinheim (2010) 53-80.

[5] N. Nitta, F.X. Wu, J.T. Lee, G. Yushin, Mater. Today 18 (2015) 252-264.

[6] J.R. Dahn, E.W. Fuller, M. Obrovac, U. von Sacken, Solid State Ionics 69 (1994) 265-270.

[7] K. Zaghib, M. Dontigny, A. Guerfi, J. Trottier, J. Hamel-Paquet, V. Gariepy, K. Galoutov, P. Hovington, A. Mauger, H. Groult, C.M. Julien, J. Power Sources 216 (2012) 192-200.

[8] W. Wang, D.W. Choi, Z.G. Yang, Metall. Mater. Trans. A, 44A (2013) S21-S25.

[9] K. Zaghib, M. Dontigny, A. Guerfi, P. Charest, I. Rodrigues, A. Mauger, C.M. Julien, J. Power Sources 196 (2011) 3949-3954.

[10] A. Jaiswal, C.R. Horne, O. Chang, W. Zhang, W. Kong, E. Wang, T. Chern, M.M. Doeff, J. Electrochem. Soc. 156 (2009) A1041-A1046.

[11] J. Gao, C. Jiang, C. Wan, Ionics 16 (2010) 417-424.

[12] A.K. Padhi, K.S. Nanjundaswamy, J.B. Goodenough, J. Electrochem. Soc. 144 (1997) 1188-1194.

[13] Y. Liu, S. Gorgutsa, C. Santato, M. Skorobogatiy, J. Electrochem. Soc. 159 (2012) A349-A356.

[14] K. Zaghib, A. Mauger, C. M. Julien, J. Solid State Electrochem. 16 (2012) 835-845.

[15] Z. Chen, I. Belharouak, Y.-K. Sun, K. Amine, Adv. Funct. Mater. 23 (2013) 959-969.

[16] M. Qin, Y. Li, X.J. Lv, Nanomaterials 7 (2017) 150.

[17] A. Mahmoud, J.M. Amarilla, K. Lasri, I. Saadoune, Electrochim. Acta 93 (2013) 163-172.

[18] P.P. Prosini, M. Carewska, C. Cento, A. Masci, Electrochim. Acta 150 (2014) 129-135.

[19] H. Buqa, M. Holzapfel, F. Krumeich, C.Veit, P.Novák, J. Power Sources 161 (2006) 617–622.

[20] S.L. Chou, Y. Pan, J.-Z. Wang, H.-K. Liu, S.-X. Dou, Phys. Chem. Chem. Phys. 16 (2014) 20347-20359.

[21] C. Fongy, P. Moreau, S. Chazelle, M. Bouvier, S. Jouanneau, D. Guyomard, B. Lestriez, J. Electrochem. Soc. 159 (2012) A1083-A1090.

[22] N. Cuesta, A. Ramos, I. Camean, C. Antuna, A.B. Garcia, Electrochim. Acta 155 (2015) 140–147.

[23] Z. Zhang, T. Zeng, C.M. Qu, H. Lu, M. Jia, Y.Q. Lai, J. Li, Electrochim. Acta 80 (2012) 440-444.

[24] S. Komaba, N. Yabuuchi, T. Ozeki, K. Okushi, H. Yui, K. Konno, Y. Katayama, T. Miura, J. Power Sources 195 (2010) 6069-6074.

[25] J.X. Li, Y. Zhao, N. Wang, Y.H. Ding, L.H. Guan, J. Mater. Chem. 22 (2012) 13002-13004.

[26] D. Versaci, R. Nasi, U. Zubair, J. Amici, M. Sgroi, M.A. Dumitrescu, C. Francia, S. Bodoardo, N. Penazzi, J. Solid State Electrochem. 21 (2017) 3429-3435.

[27] J. He, H.X. Zhong, J. Wang, L. Zhang, J. Alloys Compd. 714 (2017) 409-418.

[28] F.M. Courtel, S. Niketic, D. Duguay, Y. Abu-Lebdeh, I.J. Davidson, J. Power Sources 196 (2011) 2128-2134.

[29] Z.Q. Wang, G.J. Dang, Q.S. Zhang, J.Y. Xie, Int. J. Electrochem. Sci. 12 (2017) 7457-7468.

[30] N. Singh, C. Galande, A. Miranda, A. Mathkar, W. Gao, A.L.M. Reddy, A. Vlad, P.M. Ajayan, Sci. Rep. 2, 481 (2012).

[31] A.F. Léonard, M.-L. Piedboeuf, N. Job, Process to prepare an electrode for an electrochemical storage device. Pending Patent Application - PCT/EP2017/061786, May 17, 2017.

[32] K. Nakahara, R. Nakajima, T. Matsushima, H. Majima, J. Power Sources 117 (2003) 131-136.

[33] S.X. Zhao, H. Ding, Y.C. Wang, B.H. Li, C.W. Nan, J. Alloys Compd. 566 (2013) 206-211.

[34] ASTM D3359-97, Standard Test Methods for Measuring Adhesion by Tape Test, ASTM International, West Conshohocken, PA, (1997).

.